ChemPubSoc Europe

DOI: 10.1002/chem.201701375

CHEMISTRY A European Journal Full Paper

Enzyme Catalysis | *Hot Paper*

The Catalytic Mechanism of the Pyridoxal-5′-phosphate-Dependent Enzyme, Histidine Decarboxylase: A Computational Study

Henrique Silva Fernandes, Maria João Ramos, and Nuno M. F. S. A. Cerqueira*[a]

Abstract: The catalytic mechanism of histidine decarboxylase (HDC), a pyridoxal-5′-phosphate (PLP)-dependent enzyme, was studied by using a computational QM/MM approach following the scheme M06-2X/6–311++G(3df,2pd):Amber. The reaction involves two sequential steps: the decarboxylation of L-histidine and the protonation of the generated intermediate from which results histamine. The rate-limiting step is the first one ($\Delta G^{\neq} = 17.6$ kcal mol^{-1}; $\Delta G_r = 13.7$ kcal mol^{-1}) and agrees closely with the available experimental k_{cat} (1.73 s^{-1}), which corresponds to an activation barrier of 17.9 kcal mol^{-1}. In contrast, the second step is very fast ($\Delta G^{\neq} = 1.9$ kcal mol^{-1}) and exergonic ($\Delta G_r = -33.2$ kcal mol^{-1}). Our results agree with the available experimental data and allow us to explain the role played by several active site residues that are considered relevant according to site-directed mutagenesis studies, namely Tyr334B, Asp273A, Lys305A, and Ser354B. These results can provide insights regarding the catalytic mechanism of other enzymes belonging to family II of PLP-dependent decarboxylases.

Introduction

Histamine (2-(1*H*-imidazole-4-yl)ethanamine) is a biological amine produced by the body during an allergic reaction and is also important in the central nervous system, stomach, cardiovascular system, and smooth muscle. Several physiological events are attributed to histamine, such as cell cycle arrest,[1] muscle endurance,[2] hair growth,[3] and histamine-containing granule maturation.[4] The critical physiological and pathological role played by histamine makes it further important in many illnesses, for example atopic dermatitis,[5] chronic allergic contact dermatitis,[6] allergic rhinitis,[7] gastric ulcer,[8] diabetes,[9] chronic heart failure,[10] and several types of cancer.[11]

Taking into account the importance of histamine in human health, several studies have been conducted to gain a better understanding of how it is produced and catabolized by cells.

In eukaryotes, histamine is produced from the decarboxylation of L-histidine into carbon dioxide by L-histidine decarboxylase (HDC, EC 4.1.1.22; Figure 1).[12] HDC is an active homodimer that contains two active sites at the interface of both monomers, each one containing residues from the other subunit (Figure 2, right).[13] Each active site shelters one molecule of the pyridoxal-5′-phosphate (PLP) cofactor, an active form of vitamin B_6 that is essential for the catalytic process.[14] The PLP cofactor binds to the active site during the dimerization process where it becomes covalently bonded to an active site lysine (Lys305A) through an imine linkage. This intermediate is often identified as the internal aldimine[15] and ensures that the PLP cofactor is properly placed at the active site to make it ready to react with the substrate. When the substrate (L-histidine) is available in the active site of HDC, it binds to the PLP cofactor. In this process, the imine bond formed between PLP and Lys305A is cleaved and a new one is created between the PLP cofactor and the amino group of the substrate. This new intermediate is frequently known as the external aldimine.[15]

The formation of the internal and external aldimines, which is common to all PLP-dependent enzymes, has already been extensively studied and characterized by low energetic profiles that allow the enzyme to easily interchange between each of these intermediates[16] (Figure 1). The chemical reactions that occur after the formation of the external aldimine are what distinguish the specific chemistry that is catalyzed by each PLP-dependent enzyme. In the case of HDC, the enzyme catalyzes a decarboxylation reaction, and this is the main topic of this article.

The wild-type form of HDC catalyzes the decarboxylation process in a very efficient way ($k_{cat}/K_M = 17.3$ s^{-1} mM^{-1}) and the full process is characterized by a reaction rate (k_{cat}) of 1.73 s^{-1}.[12a]

In the last five years, mutagenic studies have pinpointed several residues that play an active role during catalysis. Generally, based on these observations, there is a consensus that the reaction proceeds in two sequential steps. First, the decarboxylation process, which results in the formation of one carbon dioxide molecule, occurs followed by generation of a quinonoid intermediate. Subsequently, the protonation of this reaction in-

[a] H. S. Fernandes, Dr. M. J. Ramos, Dr. N. M. F. S. A. Cerqueira
UCIBIO-REQUIMTE, Departamento de Química e Bioquímica
Faculdade de Ciências s/n, Universidade do Porto
4169-007 Porto (Portugal)
E-mail: nscerque@fc.up.pt

Supporting information and the ORCID identification numbers for the authors of this article can be found under https://doi.org/10.1002/chem.201701375.

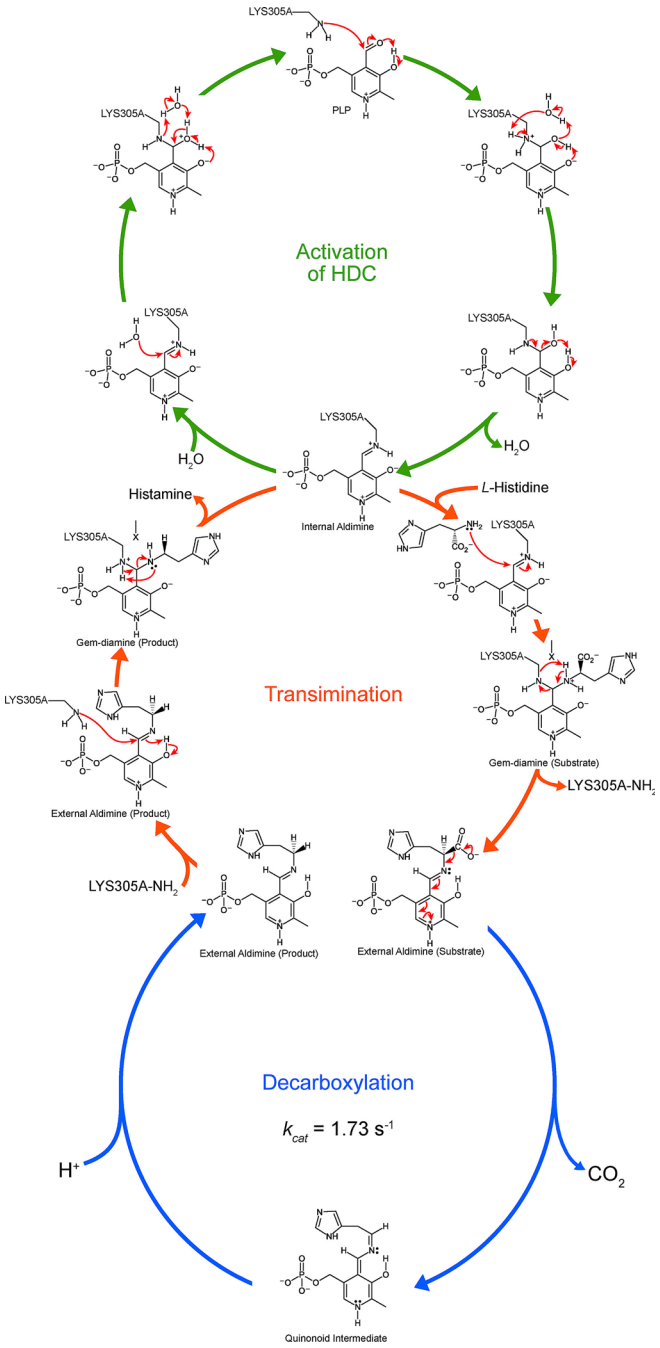

Figure 1. Schematic representation of the currently accepted mechanism for the internal and external aldimine formation for PLP-dependent enzymes[16] and also the specific reaction catalyzed by the HDC.

termediate takes place, and the product of the reaction (histamine, but still bonded to the PLP cofactor) is generated.

In 2008, Moya-Garcia et al. studied, by computational means, the first step of the catalytic mechanism of HDC using a homology model of HDC that was built based on two incomplete crystallographic structures of aromatic-L-amino-acid decarboxylase (AADC) (PDB IDs: 1JS3 and 1JS6).[17] In the study, the authors proposed that this step should be the rate-limiting one since it was characterized by a high activation energy of 20.4 kcal mol^{-1}. However, neither the product of the reaction of the first step nor the second step of the reaction was described, which makes this study incomplete. In addition, in 2012, the X-ray structure of HDC was determined for the first time (PDB ID: 4E1O). This new structure of the enzyme revealed that the homology model presents several limitations in the region of the active site. For example, in the X-ray structure, the carboxylate group of the substrate is pointing towards the solvent, whereas in the homology model it is pointing in the opposite direction (Figure 2, right). The homology model also lacks a network of hydrogen bonds that surround the PLP cofactor, which were found to be important to stabilize it during the catalytic process. The computed energies for the decarboxylation process are also higher than would be expected when taking into account the reaction rate that was determined experimentally.

The available experimental data regarding HDC provides important information on several snapshots of the catalytic mechanism. In particular, it is possible to follow, by UV/Vis spectroscopy, the formation of the external and internal aldimines.[12a,15] The available site-directed mutagenesis studies also allow identifying the active site residues that play an important role during catalysis. Mutations of Lys305A by alanine,[18] glycine[19] or arginine[20] completely inactivate the enzyme. This residue is the one that becomes covalently bonded to the PLP cofactor when the internal aldimine is generated, and thus important to make the enzyme ready to react with the substrate. Mutation of Asp273A by glycine likewise leads to a complete inactivation of the enzyme. Asp273A makes an important hydrogen bond with the pyridine ring of PLP and helps the stabilization of the cofactor inside the active site. Mutation of His194A or Ser304A by glycine almost inactivates the enzyme. His194A makes a π-stacking interaction with the PLP ring system, and is important for the correct orientation and alignment of the PLP inside the active site of the enzyme[19] (Figure 2, right). Ser304A interacts closely with Lys305 by a hydrogen bond and it is proposed to be important for the correct alignment of this residue that is essential for the formation of the internal aldimine.[19] Mutations of Tyr84A, Tyr80A, or Ala86A by glycine are also described to negatively influence the enzymatic activity of HDC,[19] and the new X-ray structure shows that they are important for stabilizing the substrate inside the active site.[12a] Fleming et al. have further reported that mutation of several amino acid residues in the loop located in the top region of the active site, interferes with the HDC activity. In particular, mutation of Tyr334B by glycine leads to a complete loss of the enzymatic activity, whereas mutation of the neighbor residues decreases the catalytic activity of the enzyme. This loop protects the active site from the solvent and is expected to play an active role during the formation of histamine after the decarboxylation process takes place.[12a] All of these facts suggest that the mechanism of HDC may be different from the one previously proposed by Moya-Garcia et al.[17a]

Here, we have studied the catalytic mechanism of HDC with an atomic level of detail by computational approaches. We intend to revise the reaction mechanism that is proposed for HDC taking into account the new X-ray structure and, therefore, the new orientation of the external aldimine with the

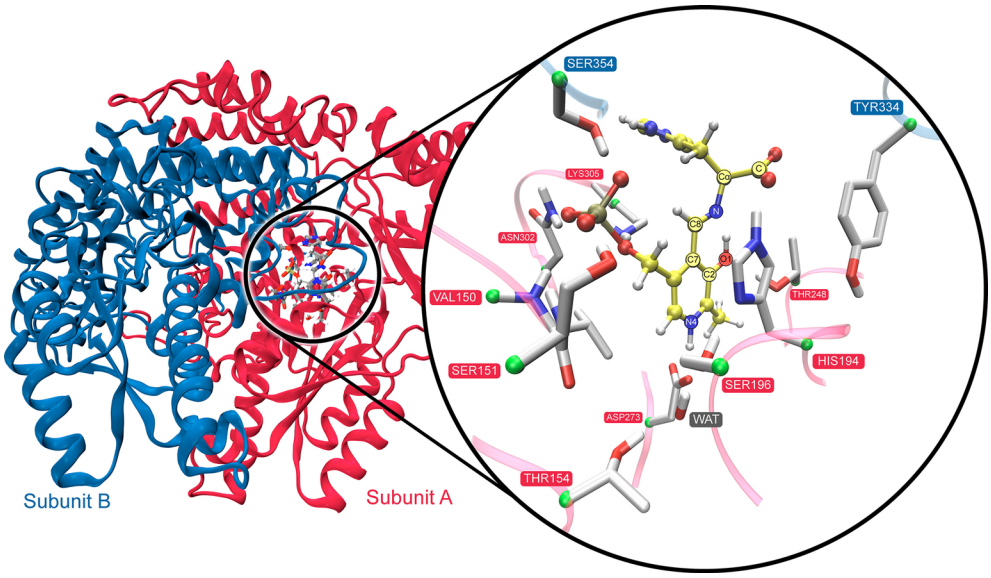

Figure 2. (Left) New cartoon representation of the X-ray structure of HDC from *Homo sapiens* (PDB code 4E1O), with the external aldimine (PLP cofactor bonded to the L-histidine). Subunits A and B are colored in red and blue, respectively. (Right) Representation of the atoms that were placed in the HL layer during the geometry optimizations. The carbon atoms from amino acid residues and the water molecule are colored in gray whereas the external aldimine ones are colored in yellow. The hydrogen atoms bonded to nonpolar atoms belonging to amino acid residues are not represented to simplify the representation. The green spheres represent the hydrogen atoms that were used as link atoms.

substrate bonded to it. In addition, we report, for the first time, the second step of the catalytic process. This step involves the protonation of the quinonoid intermediate that is generated after the decarboxylation process and the subsequent formation of histamine. To date, nothing is known about this reaction and there are not even hints about which active site residue is responsible for the protonation of the quinonoid intermediate. Therefore, this study provides, for the first time, the complete description of the catalytic mechanism of the HDC.

Computational Details

Preparing the structures

The crystallographic structure (PDB ID: 4E1O) used in this study has three equivalent dimeric structures (dimers AB, CD, and EF). Among the three dimers, dimer AB (Figure 2) was chosen because it presents a less distorted structure of the external aldimine and it does not have any artificially introduced tag of amino acid residues. The dimer has two active sites, and one of them was chosen to study the catalytic mechanism. This corresponds to the one that belongs to chain A. Since this structure was obtained through the co-crystallization of HDC with L-histidine methyl ester inhibitor (HME), we removed the methyl group bonded to the carboxylate group, from that inhibitor, to obtain the structure of the natural substrate (L-histidine; Figure 5). Additionally, we mutated two serine residues from each subunit (Ser180 and Ser418) to cysteine because they were mutated by the experimentalists in order to help the crystallization process. These two residues are far from the active site and do not affect the catalytic efficiency.[12a,21] The same protocol was used to build the quinonoid intermediate, but deleting instead the methyl group and the carboxylate group from the external aldimine available in the PDB, with the HME inhibitor.

Molecular dynamics simulations

The protein and the external aldimine or quinonoid intermediate were solvated by using TIP3P[22] type water molecules. The water box was constructed allowing a minimum distance of 12 Å from protein to each face of the box. Hydrogen atoms were added to the model using SANDER from the AMBER12 package.[23] In this work, we considered the protonation states for all amino acids at pH 7.0 according to PROPKA 3.1.[24] The parameterization of the external aldimine and quinonoid intermediate were carried out through an optimization using the Hartree–Fock (HF/6-31G(d)) method to depict the atomic charges and the antechamber software from AMBER12 package[23] to assign the atom types. In the Supporting Information, the frcmod., prepc., and lib. files containing the topology and parameters of these structures are available for inspection.

After performing molecular dynamics (MD) simulations with the previous models, average structures from the most representative clusters originated in the MD simulations were selected to perform further calculations or to give hints about the catalytic process. In this case, one structure of the model with the external aldimine and two structures for the model with the quinonoid intermediate were selected. The MD simulation of HDC with the quinonoid intermediate was carried out to search possible candidates for proton donors that can protonate the quinonoid intermediate during the second step.

The MD simulations were made with the AMBER12 software[23] using a NPT ensemble (GAFF[25] and ff99SB[26] force fields, 60 ns, 310.15 K, Langevin thermostat,[27] 1.0 bar, integration step of 1 fs, non-bond interaction cut-off of 10.0 Å).

QM/MM

The QM/MM model included the full dimer, the external aldimines in each active site, and all the water molecules located at a maximum of 2 Å from the protein. All atoms positioned more than 30 Å

away from the active site were fixed during the geometry optimizations.

Given that the system is very large (more than 17000 atoms) and the geometry optimizations are very time-consuming, we used the ONIOM[28] method to perform the calculations. This method allows the division of a system in several regions that are treated by using different theoretical levels. In this work, we divided the entire system into two regions: the high-level (HL) layer treated with density function theory (DFT); and the low-level (LL) layer using with molecular mechanics (MM). The HL layer included the external aldimine plus the relevant amino acid residues in one of the active sites. The amino acid residues that were included in the HL layer changed depending on the hypothesis that was tested and, therefore, will only be focused on in the discussion section. The remaining atoms were included in the LL layer of the system. We used hydrogen atoms as link atoms to complete the valence of the bonds spanning between the two layers of our ONIOM QM/MM Scheme (Figure 2, right). The geometry optimization of the HL layer was made with DFT and the B3LYP functional.[29] This functional was chosen due to its very good results in the study of biological systems.[30] The 6-31G(d) basis set was employed as implemented in Gaussian 09.[31] In order to explore the reactional space, some conformations of the external aldimine and amino acid residues were tested through linear transit scans along the reaction coordinates implicated in each studied reaction. Subsequently, the transition states (TS) were fully optimized, starting from the structure of the higher energy point of the scans. The reactants and products were determined through internal reaction coordinate (IRC)[32] calculations. The transition states (TSs) were also verified by vibrational frequency calculations, having solely one imaginary frequency with the correct transition vector. The minima were also submitted to vibrational frequency calculations and no imaginary frequencies were assessed in the entire system. The ZPE, thermal, and entropic energy corrections were calculated at 310.15 K and 1.0 bar during the frequency calculation of each minima and TS. Gaussian provides a thermochemistry section in every output from a frequency calculation, which has data about ZPE, and thermodynamics energies, enthalpies and Gibbs free energy.[33]

The ΔS results from the sum of several contributions: rotational, translational, electronic, solvation, and vibrational. The rotational and translational contributions were calculated through classic approximations using the rigid rotor and the particle in the box models, respectively. The vibrational has the greatest contributions which were also computed during the frequency calculations. No excited state was studies in this work therefore the electronic contribution is zero. The solvation contribution was not calculated since we do not expect significant modifications of the solvation during the course of each reaction independently, and the calculation of this contribution requires a huge sampling that would not result in more accurate results.

At the end, the energies of the minima and the TS were calculated by using a more complete basis set, 6–311++G(3df,2pd), a correction term for dispersion interactions (GD3),[34] and also the functional M06-2X, for the HL layer. The results demonstrate that there are no substantial differences in the calculated energies with and without the inclusion of the dispersion effect (the energetic difference between both calculations is below 0.2 kcal mol^{-1}).

With respect to the interaction between the LL and HL layers, mechanical embedding was used due to the hardware limitations considering the system's size. The activation and reaction energies presented here were calculated through the difference between the Gibbs free energies of TS and reactant, or product and reactant, respectively.

The atomic charges analyses of the QM layer of the QM/MM model were calculated considering Merz–Singh–Kollman charges.[35]

Visual molecular dynamics (VMD)[36] and GaussView 5.0[37] were used as visualization tools.

Results and Discussion

The recent proposal, in the literature, on the catalytic mechanism of HDC is still insufficient to understand how the catalytic process occurs. This happens because only very recently it was possible to solve the crystal structure of this enzyme. Moreover, this recent proposal is based on a homology model in which the orientation of the substrate inside the active site is not what is found in the recent X-ray structure of the enzyme. This means that the catalytic mechanism of HDC needs to be revised in light of the most recent data.

The model used here to study the catalytic mechanism relies on the recent X-ray structure of HDC, in which HDC is co-crystalized with an inhibitor bound to the PLP cofactor through an imine linkage. Since the reaction intermediate that precedes the decarboxylation process (the first step of the mechanism) is an external aldimine, in which the substrate is covalently bound to the PLP cofactor by an imine linkage (PLP + L-histidine), we started by correcting the external aldimine that exists in the PDB structure with the inhibitor (PLP + HME) with the one containing the natural substrate (PLP + L-histidine).

To accommodate all the changes made to the substrate and improve the hydrogen bond network between the cofactor and the residues of the binding site, we submitted the structure to an MD simulation. We have also performed a second MD simulation with the product of the decarboxylation process, the quinonoid intermediate. This was done to gather additional insight regarding the possible rearrangement of the residues of the active site after the decarboxylation process occurs. This was later found to be useful for obtaining additional information on the role played by several active site residues during the decarboxylation process and in the following reactions.

In the next section, the results obtained from the MD simulations are discussed. Subsequently, QM/MM results are presented, and the energetic profiles of the studied reactions are described in detail.

Molecular dynamics simulations

The MD simulation of the enzyme with the external aldimine containing the substrate was carried out for 60 ns. The RMSd analysis did not present any abnormal fluctuation, and the equilibrated region (last 20 ns) presents a low RMSd value of 1.86(±0.06) Å (Figure 3). The same trend was also observed for each subunit individually, which present almost the same RMSd (subunit A: 1.87(±0.06) Å; subunit B: 1.67(±0.08) Å).

A cluster analysis was then conducted in the equilibrated region of the MD simulation, and the most representative structures were analyzed and considered for the subsequent ONIOM calculations. All these structures show some interactions that are ubiquitous among all MD simulation. For exam-

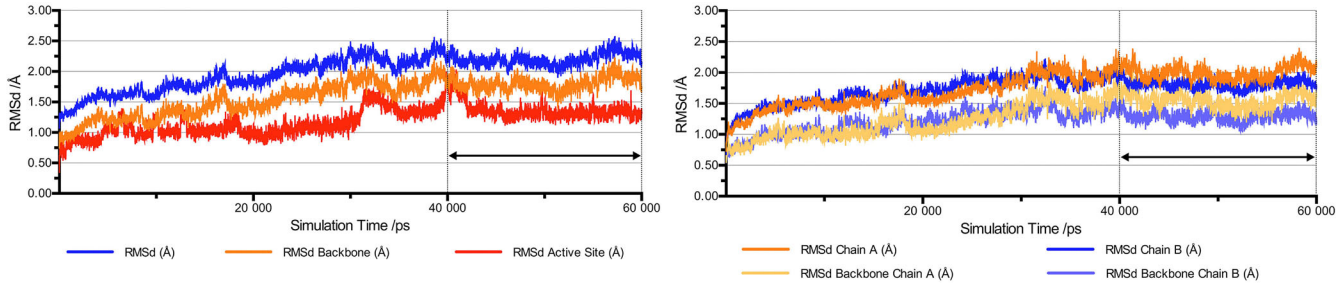

Figure 3. RMSd values for the MD simulation of HDC with external aldimine. (Left) The blue, orange, and red lines correspond to the RMSd values of all atoms in the system, only the backbone, or the active site amino acid residues plus the external aldimine, respectively. (Right) The orange lines correspond to the RMSd values of the amino acid residues of the subunit A, whereas the blue ones relate to the amino acid residues of the subunit B. The system was considered equilibrated during the last 20 ns.

ple, amino acid residues Ser151A, Val150A, Asn302A, Ser354B, and Lys305A are responsible for stabilizing the phosphate group of PLP cofactor, through several hydrogen bonds, and anchor it inside the active site (Figure 2, right). The position of the pyridine ring of the PLP cofactor is also stabilized by a strong hydrogen bond provided by Asp273A, as well as by the imidazole ring of His194A with which it interacts by π-stacking. A conserved network of hydrogen bonds is also observed in the active site that interconnects Asp273A, a water molecule, Ser196A, His194A and the carboxylate group of the substrate (Figure 2, right).

The main difference between all the structures collected from the MD simulation is the position of the amino acid residues belonging to the flexible loop that closes the active site. Among these residues, Tyr334B (Figure 2, right) is the one presenting a higher flexibility.

A similar protocol was carried out for the MD simulation of the enzyme with the quinonoid intermediate. The MD simulation ran for 60 ns, and the system was considered equilibrated during the last 20 ns with an RMSd value of 2.11(±0.11) Å (Figure 4). From the MD simulation analysis, His194 and Tyr334B were selected as strong candidates to perform the protonation of the quinonoid intermediate that occurs after the decarboxylation process.

QM/MM studies

We established the catalytic mechanism of HDC resorting to QM/MM studies, which will be described clearly next. However, other attempts and calculations have been performed that we chose to present in Supporting Information since they will be of interest only to the more computationally orientated reader.

Conformation of the external aldimine

The catalytic mechanism of HDC was initially studied by resorting to QM/MM methodologies with one structure that was retrieved from the most representative set of snapshots of the MD simulation. In this structure, L-histidine (substrate; Figure 5, center) retains the same conformation of the inhibitor in relation to the PLP cofactor, as it is observed in the co-crystalized X-ray structure 4E1O (Figure 5, left). Such conformation is not common among the PLP dependent enzymes since in these systems the NH group of the imine linkage is pointing towards the ketone group and not to the phosphate group as it is found in this X-ray structure. This suggests that such a configuration could be a consequence of the inhibitory process. However, since the inhibitor is very similar to the natural substrate and only differs on a methyl group, this new configuration could be an intrinsic characteristic of the enzyme and important for the catalytic process. Taking this into account, we started our study investigating the decarboxylation process with the external aldimine adopting the uncommon configuration observed in the co-crystalized X-ray structure 4E1O.

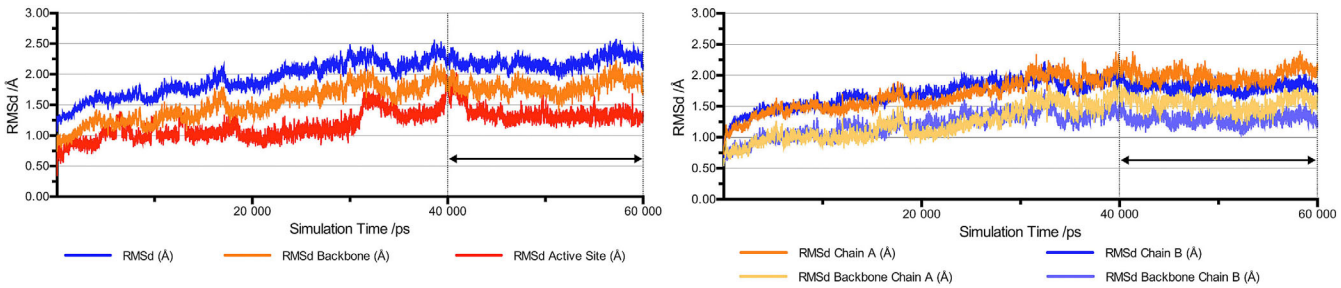

Figure 4. RMSd values for the MD simulation of HDC with the quinonoid intermediate. (Left) The blue, orange, and red lines correspond to the RMSd values of all atoms in the system, only the α-carbons, or the active site amino acid residues plus the quinonoid intermediate, respectively. (Right) The orange lines correspond to the RMSd values of the amino acid residues of the subunit A, whereas the blue ones relate to the amino acid residues of the subunit B. The system was considered equilibrated during the last 20 ns.

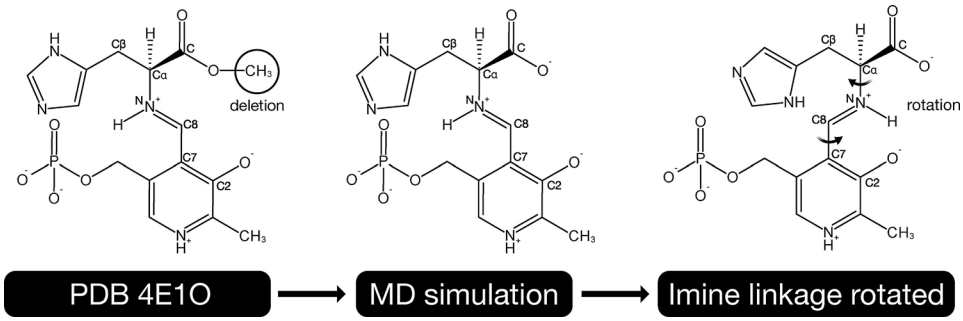

Figure 5. Structures of the external aldimine (Left) available in the PDB file 4E1O where the PLP cofactor is bound to the HME inhibitor; (Center) where the PLP cofactor is bound to the natural substrate; (Right) where the imine linkage was re-orientated to fit the common configuration of other PLP-dependent enzymes.

The QM/MM studies revealed that the decarboxylation cannot occur under physiological conditions with the external aldimine adopting the uncommon configuration. The calculated activation and reaction energies are very high (28.9 and 28.5 kcal mol^{-1}, respectively) and much higher than the one expected taking into account the experimental k_{cat} (which points to 17.9 kcal mol^{-1}).[12a]

We also tested other possible rearrangements of the external aldimine and the surrounding active site residues to determine which conformations are prohibited for the reaction to occur. A detailed description of these attempts and the respective activation and reaction energies can be found in Supporting Information (detailed description of the alternative mechanisms studied in this work).

Facing these results, we studied the decarboxylation process using the external aldimine in a conformation that is generally adopted by the PLP-dependent enzymes. To this end, we used the same structure that was retrieved from the MD simulation and rotated the two dihedral angles involved in the imine linkage by 180° (C2-C7-C8-N and C8-N-C2-C; Figure 5, right). This new conformation of the external aldimine fits very well inside the active site and does not imply additional rearrangements of the neighbor active site residues. This new conformation also allows the keto-enol tautomerism between the protonated nitrogen from the imine linkage and the ketone group of the PLP cofactor as it has been proposed by spectroscopic studies.[15] The calculated free energies for the decarboxylation process using this structure agrees very well with the experimental k_{cat} and are described in the next sections.

Decarboxylation of L-histidine

The QM/MM study was conducted by considering all the protein (active dimer), a water coat of 2 Å and the two external aldimines placed in the two active sites. The HL layer included the external aldimine placed in the active site of subunit A, the sidechain of amino acid residues His194A, Ser196A, Thr154A, Thr248A, Asp273A, Ser151A, Asn302A, and Lys305A, a water molecule, and the complete amino acid residue Val150A (Figure 6). The system had a total of 17392 atoms from which 128 were considered in the HL layer.

In the reactant of this reaction, the carboxylate group of the substrate is perpendicular to the conjugated system of PLP cofactor, and it is pointing and interacting with His194A by a hydrogen bond (1.63 Å). His194A, together with Ser196A and a water molecule, close a network of hydrogen bonds between the amino acid residue Asp273A and the carboxylate group of the substrate which was found to be important for the catalytic process. The Asp273A residue is negatively charged and it stabilizes the protonated and positively charged nitrogen of the pyridine ring of the PLP cofactor (1.52 Å) but the proton transfer never occurs. The imidazole group of the substrate is stabilized by an important hydrogen bond that is endorsed by Ser354B (1.73 Å). The phosphate group of the PLP cofactor has a charge of −2 and it is extensively stabilized by a network of hydrogen bonds endorsed by Ser151A (–OH: 1.64 Å; NH: 2.64 Å), Val150A (NH: 2.47 Å), Asn302A (–NH_2: 2.18 Å), Ser354B (–OH: 1.51 Å), and Lys305A (–NH_2: 2.45 Å).

In the course of the decarboxylation process, the Cα–C bond becomes weaker, promoting the decarboxylation and the release of the carbon dioxide. The TS of this reaction is characterized by only one imaginary frequency at 87.2 cm^{-1}, in which the interatomic distance between the Cα and C carbons is 2.73 Å. (Figure 6). At the end of the decarboxylation process, one molecule of carbon dioxide is formed, and it is released from the active site (Supporting Information, Figure S1). At the same time, a quinonoid intermediate is generated.

After the decarboxylation process takes place, an electronic-withdrawing effect is observed that is mediated by the conjugated system of the PLP cofactor. The negative charge in the reactants is concentrated on the carboxylate group and, in the product of the reaction, is accommodated on the PLP cofactor (−1.18 a.u. in the reactant versus −1.72 a.u. in the product) and in particular at the nitrogen N4 belonging to the pyridine ring (−0.35 a.u. in the reactants versus −0.53 a.u. in the product). This effect is confirmed by a decrease in the bond length of N4–H (1.10 Å in the reactants versus 1.06 Å in the product) and the consequent increase of the distance between Asp273A and the N4–H of the PLP cofactor (1.52 Å in the reactants versus 1.64 Å in the product). In order to compensate the negative charge of Asp173A during this charge transfer effect, the interaction of this residue with the neighbor water molecule is strengthened (1.81 Å in the reactants versus 1.77 Å in

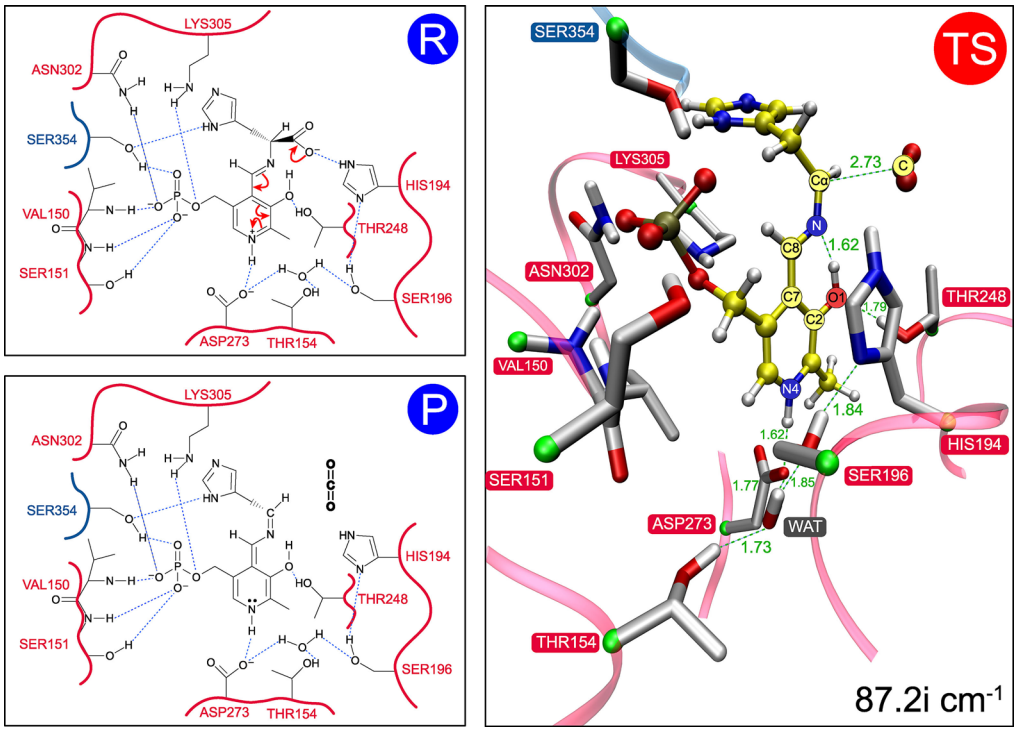

Figure 6. Structures of reactant, TS, and product of the first step of the reaction catalyzed by HDC. (Left) Wedge-Dash representation of the structures of reactant and product. (Right) New cartoon and licorice representations of the TS structure of the active site.

the product). At the same time, the hydrogen bond established between Ser196A and His194A becomes weaker (1.77 Å in the reactants versus 1.87 Å in the product) since Ser196A is pushed by this water molecule that interacts with the Asp273A amino acid residue.

Our calculations also reveal alterations in the conjugated π-system along the PLP cofactor, during the charge transfer effect. Two double bonds are formed between the Cα–N and the C6–C7 atoms because their length decreases from 1.45 and 1.48 Å in the reactant to 1.31 and 1.40 Å at the product, respectively. At the same time, the double bond C8=N becomes single (1.29 Å in the reactants versus 1.37 Å in the product). These results indicate that the negative charge is delocalized along these three bonds, but it is not accommodated here since the charge variation at this position of the PLP is almost insignificant (+0.06 a.u.). The carbon Cα acquires an sp^2 configuration, becoming co-planar with its adjacent atoms (carbon Cβ, hydrogen Hα, and nitrogen N). As expected, no significant changes are observed with respect to the amino acid residues that are stabilizing the phosphate group of PLP cofactor.

The calculated energetic profile for the decarboxylation process is very favorable (E_a = 17.1 kcal mol^{-1}, and E_r = 16.9 kcal mol^{-1}) and in agreement with the experimental k_{cat} (17.9 kcal mol^{-1}). In addition, the energy of the HL layer is the one that contributes more to the total energy of the QM/MM model, and the contribution of the LL layer is almost negligible. Single point energy calculation (ONIOM(M06-2X/6-311++G(3df,2pd):AMBER)) together with thermal corrections and corrections for dispersion interactions reveal that the decarboxylation process is characterized by a free activation energy of +17.6 kcal mol^{-1} and it is endergonic in 13.7 kcal mol^{-1}. The energetic profile of this reaction indicates that during the reaction, the entropy has a preponderant effect decreasing the activation barrier in 3.6 kcal mol^{-1} and the reaction energy in 5.0 kcal mol^{-1}.

Protonation of the quinonoid intermediate

Once the formation of carbon dioxide is complete, it leaves the active site, and the PLP cofactor remains covalently bound to the decarboxylated histidine through an imine linkage. This reaction intermediate is commonly known as the quinonoid intermediate that is negatively charged and characterized by an extended conjugation π-system.

The next step of the catalytic mechanism involves the protonation of carbon Cα from which results the external aldimine, in which the PLP cofactor is bound to the product of the reaction, histamine. It is known that the proton that is required for such reaction comes from the solvent, but as the active site is not freely solvent accessible there must be an amino acid that catalyzes this process. Since there are no hints about which residues could protonate the quinonoid intermediate, we tested the two hypotheses that emerged from our MD simulations.

The MD simulations performed with HDC and the quinonoid intermediate show that the loop located in the top region (containing amino acid residue Tyr334B) of the active site precludes any direct interaction of the quinonoid intermediate with the solvent. The cluster analysis obtained from the last 20 ns of the MD simulations reveal that His194A and Tyr334B

are close to carbon Cα. From these two residues, Tyr334B is more likely to be involved in the proton transfer because it is located in a flexible loop that is exposed to the solvent. However, the participation of His194A in this process cannot be disclosed because it establishes an important hydrogen bond with Tyr334B and can, therefore, mediate this process.

Based on the QM/MM structure of the product of the first step, two hypotheses were studied concerning the second step.

In one model, His194A mediates the proton transfer from Tyr334B to carbon Cα of the quinonoid intermediate (Figure 7, hypothesis His-Tyr). In the second one, Tyr334B is directly involved in the proton transfer through a water molecule that shuttles the proton to the carbon Cα of the quinonoid intermediate (Figure 7, hypothesis Wat-Tyr).

The system used to study the second step is identical to the one used to study the decarboxylation reaction, however, the sidechain of the amino acid residue Tyr334B was included in the HL layer, which now accounts with 140 atoms. In the case of the hypothesis Wat-Tyr, an additional water molecule was included in the HL layer (HL layer: 143 atoms).

The protonation of carbon Cα of the quinonoid intermediate by Tyr334B and mediated by His194A (Hypothesis His-Tyr) requires an activation energy of 13.8 kcal mol^{-1} and it is exothermic by 16.8 kcal mol^{-1}. The TS of this step was characterized by a unique imaginary frequency at 1517.8 cm^{-1}. However, this activation energy is prohibitive of the full reaction (first step plus the second step) under biological conditions, since the first step of the catalytic mechanisms is very endothermic and this reaction requires 13.8 kcal mol^{-1}. It means that the global activation energy of the full process would be 27.4 kcal mol^{-1}, which is much greater than the one predicted by the k_{cat} (17.9 kcal mol^{-1}) and would not be possible under physiological conditions.

On the other hand, the proton transfer from Tyr334B to carbon Cα of the quinonoid intermediate was almost spontaneous. This reaction was only possible to characterize by including a water molecule between the Tyr334 and the quinonoid intermediate. A water molecule can occupy this position because upon the release of carbon dioxide to the solvent, a free position is available in the active site that can promptly be occupied by a water molecule. The MD simulations confirm that Tyr334B is located in a loop with high mobility and in direct contact to the solvent, and therefore, it can enhance this event in the active site.

Once a water molecule enters the active site, Tyr334B can mediate the proton transfer to the quinonoid intermediate by using this water molecule as a proton shuttle.

In the reactant state, we observed the same conformation of the product from the first step. However, in this case, a water molecule occupies the region of the released carbon dioxide molecule, and one of its protons is ready for a nucleophilic attack performed by the carbon Cα of the quinonoid intermediate. The oxygen atom belonging to this water molecule is surrounded by two hydrogen bonds established with His194A and Tyr334B amino acid residues. When the reaction occurs, and the proton passes to the carbon Cα of the quinonoid intermediate, the generated hydroxyl ion is simultaneously protonated by the hydroxyl group of the Tyr334B residue.

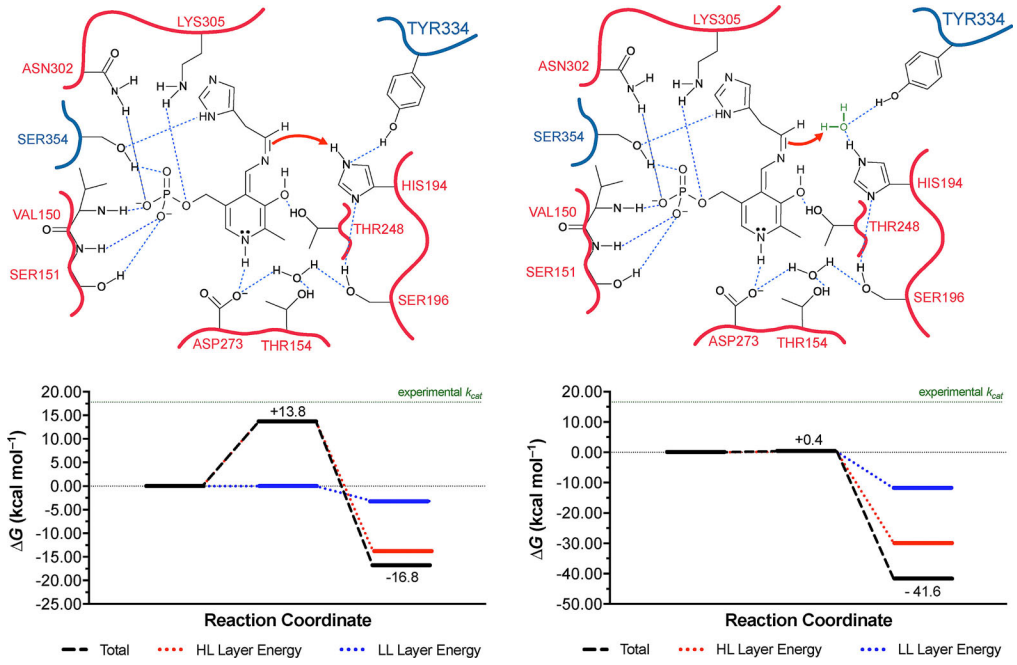

Figure 7. Hypotheses studied to characterize the second step of the catalytic mechanism of HDC. The structures colored in green correspond to those were modified comparing to the previous hypothesis. The graphs show the energetic profile for the two hypotheses. Dashed lines colored by blue represent important non-bonded interactions at the active site. Energies were calculated from the difference between the optimized TS and the reactant. No ZPE or thermal corrections were included in these calculations.

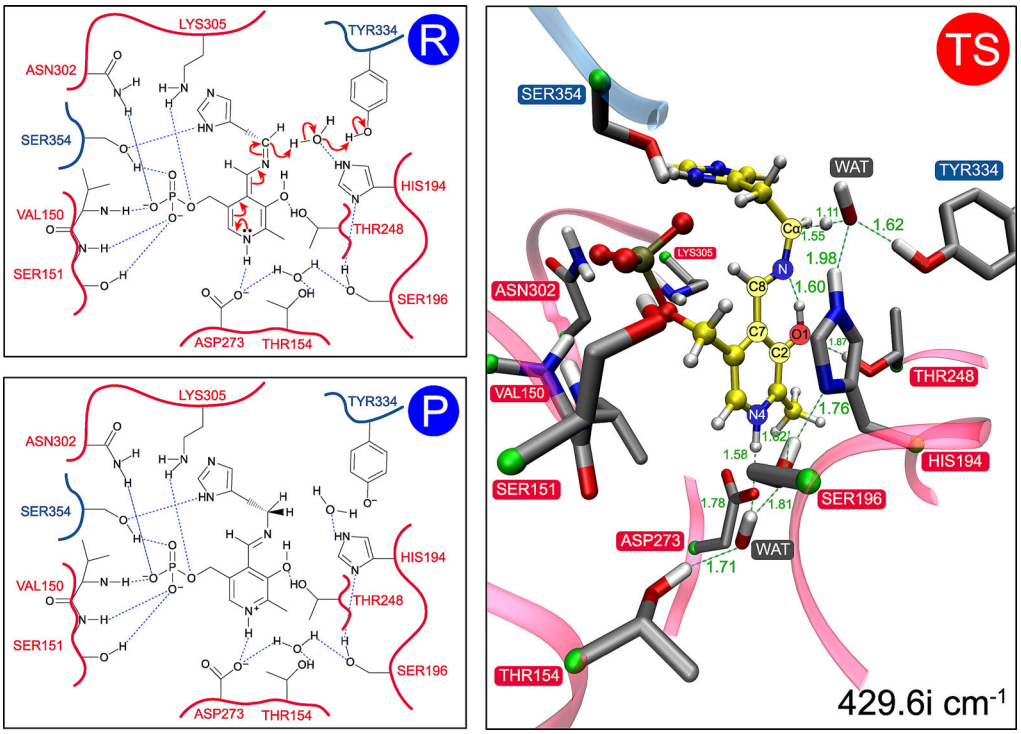

Figure 8. Structures of reactant, TS, and product of the first step of the reaction catalyzed by HDC. (Left) Wedge-Dash representation of the structures of reactant and product. (Right) New cartoon and licorice representations of the TS structure of the active site.

The energetic profile of this reaction was calculated and all the minima were characterized including the TS which has solely one imaginary frequency at 429.6 cm^{-1} (Figure 8). This reaction is very favorable and almost spontaneous, requiring an activation energy of 0.4 kcal mol^{-1} and it is exothermic by 41.6 kcal mol^{-1}.

From these two hypotheses, we can infer that the proton transfer mediated by Tyr334B and the water molecule is, from both kinetic and thermodynamic points of view, favored. Thermal corrections together with single-point energy calculations performed with a more accurately devised functional (M06-2X) concerning catalysis, a more complete basis set (6-311++G(3df,2pd)) and also including dispersion corrections, reveal that this reaction, requires a free activation energy of +1.9 kcal mol^{-1} and it is exergonic in −33.2 kcal mol^{-1}. These results indicate that the negative charge, which is generated during the first step, is better accommodated on Tyr334B residue rather than the quinonoid intermediate.

Although the direct participation of His194A in the protonation step can be excluded, it continues to have an important role in this step. The reaction mediated by Tyr334B and the water molecule is only possible due to the hydrogen bond that it establishes with His194A promoting, therefore, the correct position and alignment of the water molecule in relation to carbon Cα of the quinonoid intermediate and Tyr334B residue. These results are in agreement with the experimental data that show that the mutation of His194A by a glycine decreases the catalytic efficiency by almost 12 times, but it does not prevent the reaction as it does when Tyr334B residue is mutated.[19]

Once more, the PLP cofactor has a preponderant role in this reaction, but in the opposite way compared to the first step. When the first step occurs, the PLP cofactor becomes negatively charged favoring, by this way, the decarboxylation process. In the second step, the reverse process occurs and allows the charge to become lodged at carbon Cα, turning it into a better nucleophile atom to accept one proton. This process is followed by an electronic delocalization that inverts the conjugated π-system of C7, C8, N, and Cα atoms. The double bonds between C7=C8 and N=Cα atoms become single again, since the interatomic distances increase from 1.42 and 1.33 Å (reactant) to 1.48 and 1.47 Å (product), respectively. On the other hand, the single bond between C8-N atoms becomes double (1.35 Å in the reactants versus 1.28 Å in the product). Simultaneously, the quinonoid intermediate becomes less negatively charged (−1.29 a.u. in the reactant versus −1.00 a.u. in the product) and the hydrogen bond between the protonated nitrogen N4 and the carboxylate group belonging to Asp273A residue becomes stronger (1.62 Å in the reactant versus 1.50 Å in the product). As a result, the negative charge of Asp273A amino acid residue is stabilized, and the intermolecular interaction with a closer water molecule becomes weaker (1.77 Å in the reactant versus 1.81 Å in the product). At the end of the reaction, the hydroxyl group of Tyr334B residue is deprotonated and negatively charged. However, due to its exposure to the solvent, the hydroxyl group of Tyr334B residue can easily be reprotonated by a water molecule or any other acid molecule in the cell.

Conclusions

We have studied by computational means the catalytic mechanism of HDC, a PLP-dependent enzyme that catalyzes the conversion of L-histidine into histamine. The reaction was found to take place in two sequential steps. The first step is the rate-limiting one and involves the decarboxylation process (Figure 9). It requires a free activation energy of 17.6 kcal mol^{-1}, and it is endergonic by 13.7 kcal mol^{-1}. The second step involves the protonation of the quinonoid intermediate by Tyr334B with the direct participation of a water molecule and with the help of His194A. This step is almost spontaneous, requiring a free activation energy of 1.9 kcal mol^{-1}, and it is also very exergonic (−33.2 kcal mol^{-1}).

The energetic profile of the full catalytic mechanism of HDC is displayed in Figure 9. It agrees very well with the experimental k_{cat} (1.73 s^{-1}) that is equivalent to an activation barrier of 17.9 kcal mol^{-1}. In addition, the experimental evidence reveals that the enzyme cannot catalyze the reverse reaction. The calculated energies also agree with this fact since the reverse reaction requires more than 30 kcal mol^{-1} and cannot take place under physiological conditions.

All the calculations undertaken to study the catalytic mechanism of HDC were based on the only available X-ray structure of this enzyme (PDB ID: 4E1O) in which the enzyme was co-crystalized with an inhibitor (HME). The inhibitor was very similar to the natural substrate, and therefore, it was expected that the natural substrate would interact with the active site and with the PLP cofactor in a similar conformation. We have, however, found out that this is not the case.

Our calculations indicate that the orientation of the imine linkage, as it is found in the co-crystallized X-ray structure, prevents the formation of an important keto–enol tautomerism between the NH group of the amino acid substrate and the ketone group of the PLP cofactor that was found to be essential for the decarboxylation process. We propose therefore that under normal catalysis, these two groups must be pointing to the same side of the imine linkage and interacting by a hydrogen bond, similar to what is found in other PLP-dependent enzymes.[15,38] This means that the configuration of the external aldimine present in the co-crystallized X-ray structure is a consequence of the inhibitory process and should not be present under normal catalytic conditions.

We observed an important interaction between the protonated nitrogen belonging to the imidazole group of substrate and the hydroxyl group of Ser354B. The position that is occupied by this amino acid residue is known to be crucial for the control of substrate specificity of the PLP-dependent enzymes that catalyze decarboxylation reactions.[12a] What differentiates among these PLP-dependent enzymes is the side chain of their amino acid substrates, and therefore, in the case of HDC, the interaction of the side chain of L-histidine with Ser354B. This

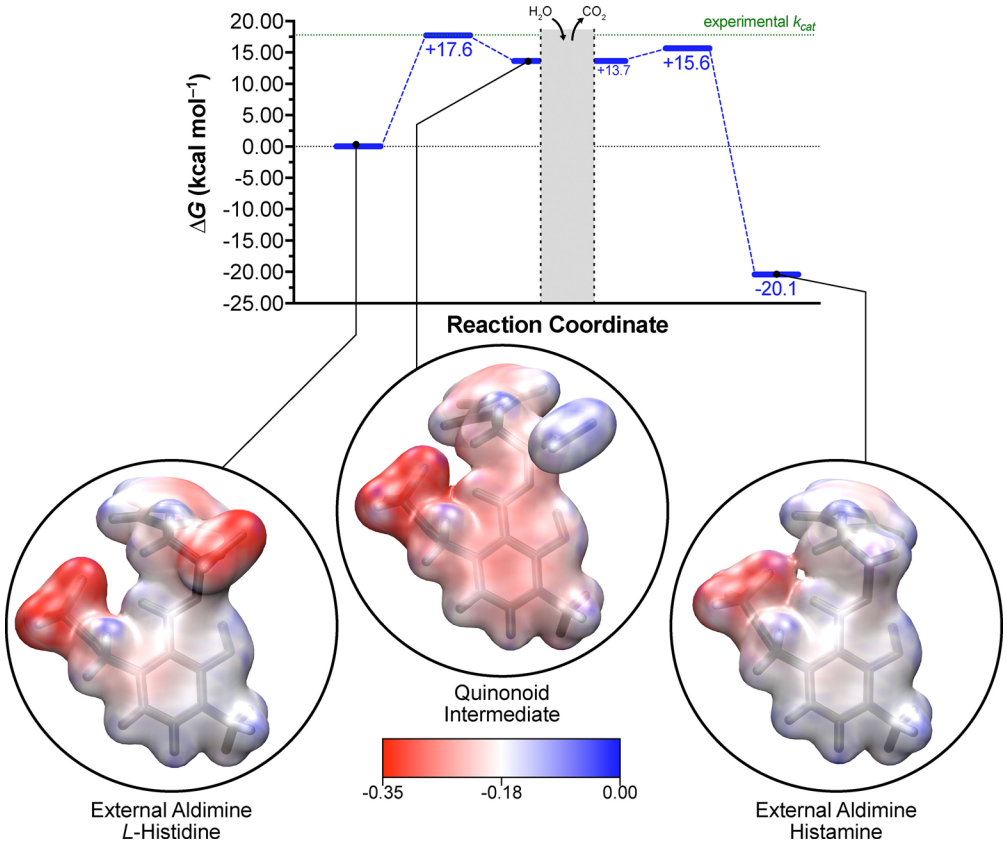

Figure 9. (Top) Energetic Profile of the catalytic mechanism catalyzed by HDC. The energy values were calculated using the following Scheme: ONIOM(M06-2X/6–311 + + G(3df,2pd):AMBER); they include the thermal corrections and the corrections for the dispersion interactions. (Bottom) Surface mapping of the Merz–Singh–Kollman charges of the external aldimines with the reactant and product and quinonoid intermediate.

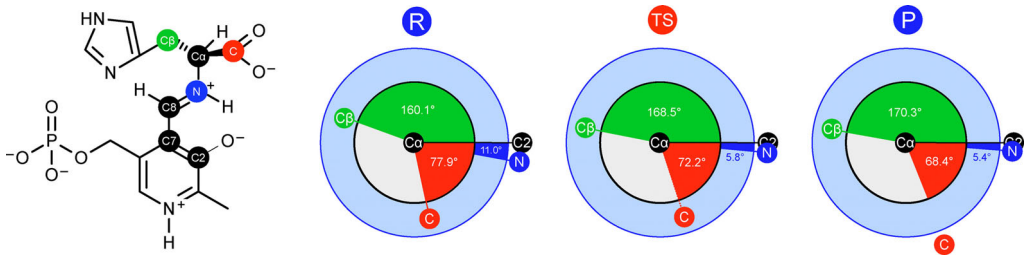

Figure 10. Analysis of the relevant dihedral angles of the reactant, TS, and product for the first step. Dihedral angles: C2-C7-Cα-C; C2-C7-Cα-Cβ; C2-C7-C8-N.

interaction should not preclude the catalytic process but should instead favor it. This is, in fact, what was experimentally observed and also what our results indicate.

Our calculations have revealed also that Tyr334B has an important role in the catalytic process but not in the decarboxylation process as it was previously suggested. This residue is located in a flexible loop that is highly exposed to the solvent and was found to be important for the protonation of the quinonoid intermediate, from which results an external aldimine in which the PLP cofactor is bonded to the product of the reaction, histamine.

We have also found an important network of hydrogen bonds involving His194A, Ser196A, a water molecule, and Asp273A that plays a key role to stabilize the negative charge of Asp273A when the PLP accommodates the negative charge of the quinonoid intermediate.

We also confirmed the described role of the PLP cofactor during catalysis, where it behaves like an electron sink. In the first step of the catalytic process, it triggers the decarboxylation process through the withdrawal of the electronic density at carbon Cα. Once the quinonoid intermediate is formed, the negative charge is accommodated through the PLP cofactor making it ready for the protonation step that takes place in the second step of the catalytic process (Figure 9). The PLP cofactor has, therefore, a double role that is fundamental for catalysis; it is able to spread the electronic density in itself, in order to cleave the bond C–Cα and promote the decarboxylation process. Simultaneously, the PLP cofactor did not kidnap the negative charge in the pyridine ring in order to make it available for the protonation of the carbon Cα, otherwise the second step could not occur.

We confirmed also, the Dunathan's effect[39] that postulates that the bond that is formed or broken during the catalytic process should be placed perpendicularly to the conjugated system of the PLP cofactor. The bond that is cleaved (Cα–C) is closer to a perpendicular position in relation to the PLP cofactor since the dihedral angle C2-C7-Cα-C is −77.9° for the reactant and −72.2° when for the TS (Figure 10).

The conclusions that were obtained in this work can also give insights about the catalytic mechanism of other enzymes belonging to family II of PLP-dependent decarboxylases. This family of enzymes includes HDC, aromatic-L-amino-acid decarboxylase (AADC; EC 4.1.1.28), and glutamate decarboxylase (GAD; EC 4.1.1.15).

The only difference that is observed in the active site among these enzymes is the residue that in HDC is occupied by Ser354B. This residue makes an important interaction with the side chain of the substrate and, therefore, it is important to modulate the specificity of the enzyme. However, we do not expect that it can affect the catalytic mechanism since this residue does not play a catalytic role.

Acknowledgements

European Union (FEDER funds POCI/01/0145/FEDER/007728) and National Funds (FCT/MEC, Fundação para a Ciência e Tecnologia and Ministério da Educação e Ciência) under the Partnership Agreement PT2020 UID/MULTI/04378/2013.UID/MULTI/04378/2013; NORTE-01-0145-FEDER-000024, supported by Norte Portugal Regional Operational Programme (NORTE 2020), under the PORTUGAL 2020 Partnership Agreement, through the European Regional Development Fund (ERDF); Fundação para a Ciência e a Tecnologia (FCT) through projects IF/01310/2013 and EXCL-II/QEQ-COM/0394/2012.

Conflict of interest

The authors declare no conflict of interest.

Keywords: computational chemistry · enzyme catalysis · histamine · histidine decarboxylase · reaction mechanisms

[1] J. Caro-Astorga, I. Fajardo, M. V. Ruiz-Perez, F. Sanchez-Jimenez, J. L. Urdiales, *Biochem. Biophys. Res. Commun.* **2014**, *451*, 580–586.
[2] F. Niijima-Yaoita, M. Tsuchiya, H. Ohtsu, K. Yanai, S. Sugawara, Y. Endo, T. Tadano, *Biol. Pharm. Bull.* **2012**, *35*, 91–97.
[3] J. I. Na, K. M. Nam, H. R. Choi, S. Inui, S. W. Youn, C. H. Huh, K. C. Park, *J. Dermatol. Sci.* **2012**, *67*, 95–100.
[4] S. Nakazawa, M. Sakanaka, K. Furuta, M. Natsuhara, H. Takano, S. Tsuchiya, Y. Okuno, H. Ohtsu, M. Nishibori, R. L. Thurmond, N. Hirasawa, K. Nakayama, A. Ichikawa, Y. Sugimoto, S. Tanaka, *Eur. J. Immunol.* **2014**, *44*, 204–214.
[5] D. Gutowska-Owsiak, L. Greenwald, C. Watson, T. A. Selvakumar, X. Wang, G. S. Ogg, *Brit. J. Dermatol.* **2014**, *171*, 771–778.
[6] K. Tamaka, M. Seike, T. Hagiwara, A. Sato, H. Ohtsu, *Exp. Dermatol.* **2015**, *24*, 280–284.
[7] G. Gervasini, J. A. Agundez, J. Garcia-Menaya, C. Martinez, C. Cordobes, P. Ayuso, J. A. Cornejo, M. Blanca, E. Garcia-Martin, *Allergy* **2010**, *65*, 1576–1584.
[8] a) P. H. Guth, P. Hall, *Gastroenterology* **1966**, *50*, 562–570; b) N. S. Parmar, G. Hennings, O. P. Gulati, *Agents Actions* **1984**, *15*, 494–499.

[9] M. Alkan, F. Machavoine, R. Rignault, J. Dam, M. Dy, N. Thieblemont, *Exp. Diabetes Res.* **2015**, *2015*, 965056.
[10] C. J. Mackins, S. Kano, N. Seyedi, U. Schafer, A. C. Reid, T. Machida, R. B. Silver, R. Levi, *J. Clin. Invest.* **2006**, *116*, 1063 – 1070.
[11] a) Y. Matsuki, A. Tanimoto, T. Hamada, Y. Sasaguri, *Modern Pathology* **2003**, *16*, 72 – 78; b) Z. Darvas, E. Sakurai, H. G. Schwelberger, H. Hegyesi, E. Rivera, H. Othsu, T. Watanabe, E. Pallinger, A. Falus, *Melanoma Res.* **2003**, *13*, 239 – 246; c) G. H. He, J. J. Lin, W. K. Cai, W. M. Xu, Z. P. Yu, S. J. Yin, C. H. Zhao, G. L. Xu, *PLoS One* **2014**, *9*, e97728; d) K. Boer, Z. Darvas, M. Baki, I. Kaszas, Z. Pal, A. Falus, *Inflammation Res.* **2003**, *52 Suppl 1*, S76-77; e) A. Tanimoto, Y. Matsuki, T. Tomita, T. Sasaguri, S. Shimajiri, Y. Sasaguri, *Pathol. Int.* **2004**, *54*, 408 – 412; f) J. Cui, G. Xu, J. Liu, Z. Pang, J. Florholmen, G. Cui, *Pathol. Oncol. Res.* **2013**, *19*, 311 – 316.
[12] a) H. Komori, Y. Nitta, H. Ueno, Y. Higuchi, *J. Biol. Chem.* **2012**, *287*, 29175 – 29183; b) L. Alcaniz, A. Vega, P. Chacon, R. El Bekay, I. Ventura, R. Aroca, M. Blanca, D. T. Bergstralh, J. Monteseirin, *FASEB J.* **2013**, *27*, 2902 – 2910; c) F. L. Pearce, *Agents Actions* **1991**, *33*, 4 – 7.
[13] a) A. A. Moya-Garcia, M. A. Medina, F. Sanchez-Jimenez, *Bioessays* **2005**, *27*, 57 – 63; b) N. Engel, M. T. Olmo, C. S. Coleman, M. A. Medina, A. E. Pegg, F. Sanchez-Jimenez, *Biochem. J.* **1996**, *320 (Pt2)*, 365 – 368.
[14] R. Percudani, A. Peracchi, *EMBO Rep.* **2003**, *4*, 850 – 854.
[15] M. T. Olmo, F. Sanchez-Jimenez, M. A. Medina, H. Hayashi, *J. Biochem.* **2002**, *132*, 433 – 439.
[16] a) N. M. Cerqueira, P. A. Fernandes, M. J. Ramos, *J. Chem. Theory Comput.* **2011**, *7*, 1356 – 1368; b) E. F. Oliveira, N. M. Cerqueira, P. A. Fernandes, M. J. Ramos, *J. Am. Chem. Soc.* **2011**, *133*, 15496 – 15505.
[17] a) A. A. Moya-García, J. Ruiz-Pernia, S. Marti, F. Sanchez-Jimenez, I. Tunon, *J. Biol. Chem.* **2008**, *283*, 12393 – 12401; b) C. Rodríguez-Caso, D. Rodríguez-Agudo, A. A. Moya-García, I. Fajardo, M. Á. Medina, V. Subramaniam, F. Sánchez-Jiménez, *Eur. J. Biochem.* **2003**, *270*, 4376 – 4387.
[18] B. A. Malcolm, J. F. Kirsch, *Biochem. Biophys. Res. Commun.* **1985**, *132*, 915 – 921.
[19] J. V. Fleming, F. Sanchez-Jimenez, A. A. Moya-Garcia, M. R. Langlois, T. C. Wang, *Biochem. J.* **2004**, *379*, 253 – 261.
[20] S. Kuramitsu, Y. Inoue, S. Tanase, Y. Morino, H. Kagamiyama, *Biochem. Biophys. Res. Commun.* **1987**, *146*, 416 – 421.
[21] H. Komori, Y. Nitta, H. Ueno, Y. Higuchi, *Acta Crystallogr. Sect. F* **2012**, *68*, 675 – 677.
[22] F. S. Tahanejad, H. Naderi-Manesh, *Eur. J. Med. Chem.* **2000**, *35*, 283 – 289.
[23] D. A. Case, T. A. Darden, T. E. Cheatham, C. L. Simmerling, J. Wang, R. E. Duke, R. Luo, R. C. Walker, W. Zhang, K. M. Merz, B. Roberts, S. Hayik, A. Roitberg, G. Seabra, J. Swails, A. W. Goetz, I. Kolossváry, K. F. Wong, F. Paesani, J. Vanicek, R. M. Wolf, J. Liu, X. Wu, S. R. Brozell, T. Steinbrecher, H. Gohlke, Q. Cai, X. Ye, J. Wang, M. J. Hsieh, G. Cui, D. R. Roe, D. H. Mathews, M. G. Seetin, R. Salomon-Ferrer, C. Sagui, V. Babin, T. Luchko, S. Gusarov, A. Kovalenko, P. A. Kollman, AMBER 12, University of California, San Francisco, **2012**.
[24] a) C. R. Søndergaard, M. H. M. Olsson, M. Rostkowski, J. H. Jensen, *J. Chem. Theory Comput.* **2011**, *7*, 2284 – 2295; b) M. H. M. Olsson, C. R. Søndergaard, M. Rostkowski, J. H. Jensen, *J. Chem. Theory Comput.* **2011**, *7*, 525 – 537.
[25] J. Wang, R. M. Wolf, J. W. Caldwell, P. A. Kollman, D. A. Case, *J. Comput. Chem.* **2004**, *25*, 1157 – 1174.
[26] V. Hornak, R. Abel, A. Okur, B. Strockbine, A. Roitberg, C. Simmerling, *Proteins Struct. Funct. Bioinf.* **2006**, *65*, 712 – 725.
[27] L. Larini, R. Mannella, D. Leporini, *J. Chem. Phys.* **2007**, *126*, 104101.
[28] a) F. Maseras, K. Morokuma, *J. Comput. Chem.* **1995**, *16*, 1170 – 1179; b) M. Svensson, S. Humbel, R. D. J. Froese, T. Matsubara, S. Sieber, K. Morokuma, *J. Phys. Chem.* **1996**, *100*, 19357 – 19363; c) S. Dapprich, I. Komaromi, K. S. Byun, K. Morokuma, M. J. Frisch, *J. Mol. Struct.* **1999**, *461*, 1 – 21.
[29] T. Yanai, D. P. Tew, N. C. Handy, *Chem. Phys. Lett.* **2004**, *393*, 51 – 57.
[30] a) N. M. F. S. A. Cerqueira, P. J. Gonzalez, P. A. Fernandes, J. J. G. Moura, M. J. Ramos, *Acc. Chem. Res.* **2015**, *48*, 2875 – 2884; b) D. S. Gesto, N. M. F. S. A. Cerqueira, P. A. Fernandes, M. J. Ramos, *J. Am. Chem. Soc.* **2013**, *135*, 7146 – 7158; c) C. Moreira, M. J. Ramos, P. A. Fernandes, *Chem. Eur. J.* **2016**, *22*, 9218 – 9225; d) R. P. P. Neves, P. A. Fernandes, M. J. Ramos, *ACS Catal.* **2016**, *6*, 357 – 368; e) E. F. Oliveira, N. M. F. S. A. Cerqueira, M. J. Ramos, P. A. Fernandes, *Catal. Sci. Technol.* **2016**, *6*, 7172 – 7185; f) A. J. M. Ribeiro, D. Santos-Martins, N. Russo, M. J. Ramos, P. A. Fernandes, *ACS Catal.* **2015**, *5*, 5617 – 5626.
[31] Gaussian 09, Revision D.01, M. J. Frisch, G. W. Trucks, H. B. Schlegel, G. E. Scuseria, M. A. Robb, J. R. Cheeseman, G. Scalmani, V. Barone, B. Mennucci, G. A. Petersson, H. Nakatsuji, M. Caricato, X. Li, H. P. Hratchian, A. F. Izmaylov, J. Bloino, G. Zheng, J. L. Sonnenberg, M. Hada, M. Ehara, K. Toyota, R. Fukuda, J. Hasegawa, M. Ishida, T. Nakajima, Y. Honda, O. Kitao, H. Nakai, T. Vreven, J. A. Montgomery, Jr., J. E. Peralta, F. Ogliaro, M. J. Bearpark, J. Heyd, E. N. Brothers, K. N. Kudin, V. N. Staroverov, R. Kobayashi, J. Normand, K. Raghavachari, A. P. Rendell, J. C. Burant, S. S. Iyengar, J. Tomasi, M. Cossi, N. Rega, N. J. Millam, M. Klene, J. E. Knox, J. B. Cross, V. Bakken, C. Adamo, J. Jaramillo, R. Gomperts, R. E. Stratmann, O. Yazyev, A. J. Austin, R. Cammi, C. Pomelli, J. W. Ochterski, R. L. Martin, K. Morokuma, V. G. Zakrzewski, G. A. Voth, P. Salvador, J. J. Dannenberg, S. Dapprich, A. D. Daniels, Ö. Farkas, J. B. Foresman, J. V. Ortiz, J. Cioslowski, D. J. Fox, Gaussian, Inc., Wallingford, CT, **2009**.
[32] K. Fukui, *Acc. Chem. Res.* **1981**, *14*, 363 – 368.
[33] J. W. Ochterski, *Thermochemistry in Gaussian*, **2000**, p. 19.
[34] a) S. Grimme, J. Antony, S. Ehrlich, H. Krieg, *J. Chem. Phys.* **2010**, *132*, 154104; b) S. Grimme, S. Ehrlich, L. Goerigk, *J. Comput. Chem.* **2011**, *32*, 1456 – 1465.
[35] U. C. Singh, P. A. Kollman, *J. Comput. Chem.* **1984**, *5*, 129 – 145.
[36] W. Humphrey, A. Dalke, K. Schulten, *J. Mol. Graph.* **1996**, *14*, 27 – 33.
[37] T. K. Roy Dennington, John Millam, 5.0.8 ed., Semichem Inc., Shawnee Mission, **2009**.
[38] H. Hayashi, H. Mizuguchi, H. Kagamiyama, *Biochemistry* **1993**, *32*, 812 – 818.
[39] a) H. C. Dunathan, *Proc. Natl. Acad. Sci. USA* **1966**, *55*, 712 – 716; b) H. C. Dunathan, *Adv. Enzymol. Relat. Areas Mol. Biol.* **1971**, *35*, 79 – 134.

Manuscript received: March 27, 2017
Version of record online: ■■ ▮▮, 0000

FULL PAPER

Role model: The catalytic mechanism of histidine decarboxylase (HDC), a pyridoxal-5′-phosphate (PLP)-dependent enzyme, was studied by using a computational QM/MM approach. The results agree with the available experimental data and allow the role played by several active site residues that are considered relevant according to site-directed mutagenesis studies to be explained.

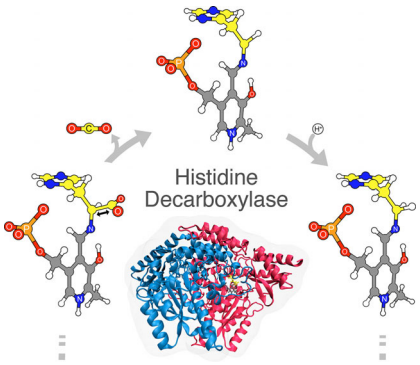

Enzyme Catalysis

*H. S. Fernandes, M. J. Ramos, N. M. F. S. A. Cerqueira**

■■ – ■■

The Catalytic Mechanism of the Pyridoxal-5′-phosphate-Dependent Enzyme, Histidine Decarboxylase: A Computational Study